Super-resolution with a complex-amplitude pupil mask encoded in the first diffraction order of a phase grating

Alberto Aguilar, Jorge García-Márquez, J.E.A. Landgrave

Version of Record: https://www.sciencedirect.com/science/article/pii/S014381662030021X
Manuscript_466e52ce79a8c45fb584bef94b171478

Super-resolution with a complex-amplitude pupil mask encoded in the first diffraction order of a phase grating

Alberto Aguilar[a], Jorge García-Márquez[b,*], J. E. A. Landgrave[c]

[a]Université de Bordeaux, Laboratoire Photonique Numérique et Nanosciences, UMR5298, F-33400, Talence, France, CNRS and Institut d'Optique, LP2N UMR 5298, F-33400, Talence, France
[b]Laboratoire National de Métrologie et d'Essais, LNE, 29, rue Roger Hennequin, 78190,Trappes, France
[c]Centro de Investigaciones en Optica, 115, Loma del Bosque, 37150, Leon, Mexico
*corresponding author jorge.garcia@lne.fr

Abstract: Diffraction imposes a barrier to resolve objects smaller than half the wavelength used to illuminate them. In optical microscopy, this barrier was surpassed 25 years ago. One form of achieving super-resolution is the use of complex-amplitude pupil masks. Spatial light modulators can be used to produce these masks, if we compensate the aberrations introduced by them. In this paper we propose a method to encode a complex-amplitude pupil mask in a phase-only spatial light modulator of the Liquid Crystal on Silicon (LCoS) variety. We describe the form in which the pupil mask is encoded in a phase grating generated with an LCoS spatial light modulator, and how the aberrations introduced by this device can also be compensated with this grating. We present numerical and experimental results that validate the method.

1. INTRODUCTION

Diffraction imposes a barrier that prevents an optical system from resolving two points closer than half the wavelength used to illuminate them [1]. Later, it was demonstrated that the minimum separation between two points to be resolved is in fact nearly a quarter of a wavelength [2]. Several efforts have been made to surpass this limitation, either in microscopy or in astronomical instrumentation. Optical super-resolving systems are conceived to cope with fundamental challenges proper to the targeted application. For instance, in microscopy, fluorescence is extensively used nowadays, and different techniques have been proposed to obtain super-resolved images with fluorescence microscopy. Examples of these techniques are Structured Illumination Microscopy (SIM) [3], deterministic functional techniques such as

STimulated Emission Depletion (STED) [4], and stochastic techniques like STochastic Optical Reconstruction Microscopy (STORM) [5]. Dyba and Hell used a Phase Mask (PhM) in a STED-4Pi microscope [6]. Since then, PhMs have been incorporated in microscopy. LCoS-SLMs have been proposed for phase measurements below the wavelength by using optical vortices [7]. More recently, spatial light modulators (SLMs) have also been incorporated in microscopy with the intention of surpassing the diffraction limit barrier [8–10]. In the case of astronomical telescopes, it has been suggested that the deformable mirrors that are used to compensate atmospheric turbulence can also be used to implement phase-only, continuous PhMs to achieve a moderate amount of super-resolution [11].

Super-resolving PhMs, also known as pupil filters or pupil masks, were originally proposed by Toraldo di Francia [12]. They were obtained in practice with two transmitting SLMs, used to synthesize a complex-amplitude (CA) PhM with two superimposed fields [14, 16] (A CA-PhM modifies both, the amplitude and the phase of an incoming beam). The new generation of SLMs, however, can exhibit phase fluctuations, a phenomenon known as flicker, preventing thus the realization of CA-PhMs with this method. This flicker depends on the electronic addressing of the signal to be displayed by the pixelated liquid crystal (LC). Then, the superposition of the fields from the two SLMs is neutralized by a biting phenomenon produced by the field fluctuations. In other words, given two SLMs acting as mirrors, each reflecting a portion of a common beam, the superposition of the two wavefronts reflected by the SLMs will be affected by non-synchronous fluctuations in phase resulting in a nullified interference pattern [17, 18]. Efforts have been made to reduce these fluctuations with polarized light [19], by cooling the LC molecules [17, 20], or by changing the period of the pulsed width modulation (PWM) of the SLMs [21].

In addition to the limitation that represents this phase fluctuation, to achieve super-resolution with SLMs the panel should be flat with an optical quality better than that imposed by Maréchal's condition [22], which is approximately of $\lambda/14$. In [23], a method to compensate the SLM panel deformations with residual errors below $\lambda/30$ was shown. This correction could not be improved further due to irregularities in the LC thickness, as described in [24]. Therefore, it is essential to calibrate the panel with a reference flat, since in this form it would be metrologically linked to a physical standard [25]; after doing this, all subsequent panel modifications could be readily detected. As explained in [23], a recursive wavefront aberration-compensation procedure with a Liquid Crystal on Silicon (LCoS) SLM can attain a high degree of correction for the +1 diffraction order of a sinusoidal phase grating recorded on it.

To avoid the effects of the phase fluctuations in SLMs, and other polarization effects [26, 27], it is desirable to attain super-resolution using only one SLM, which would have the further benefit of simplifying the setup that is used for this purpose. Despite the flicker, the polarization effects, the surface aberrations, and the spatial distribution of LC molecules, we show here that a single SLM can be used to produce a dynamic, easy-to-use, super-resolving PhM. In section 2

we describe the modulation technique that we employ for this aim, in section 3 we validate this technique with a numerical simulation, and in section 4 we describe our experimental setup and present our best results. Section 5 includes some concluding remarks.

2. COMPLEX-AMPLITUDE PUPIL MASK ENCODING

Coding a phase and amplitude mask in a spatial light modulator is done by using two SLMs, one in phase and the other in amplitude. However, some SLMs such as LCoS are dependent on the polarization of the incident beam [26, 27]. Usually, for the optimal setup using two SLMs, two different incident polarizations must be created, one for the phase and one for the amplitude and then recombine them together. However, this procedure causes unwanted depolarizing effects in the output beam. By using only one SLM working in the first diffraction order instead of two different workings in the order zero, polarization effects can be neglected, as there is no interference of two different beams with different polarizations.

One of the main advantages of using phase gratings to encode CA-PhMs is that they allow changing the diffraction efficiency at any point of its surface. As we mentioned above, one SLM was used before to generate an amplitude transmittance PhM, while a second one was used to make a phase-only PhM. As shown in [14], by superposing the outcome of both SLMs we obtain a CA-PhM. Aberrations introduced by the optical elements of a super-resolving system, however, is an important concern when making super-resolving PhMs. In optical engineering, we always look for reducing the number of elements because of several reasons: lower production costs, less raw materials, less space (compactness), to facilitate alignment, among others. This experiment was designed considering all these design parameters. Polarization, flicker, and LC-SLM intrinsic aberrations could be avoided with a CA-PhM embedded in a single SLM. Taking advantage of this, we decided to encode the CA-PhM in the field produced by the phase gratings in their +1 diffraction order.

Let us suppose that a modulated phase grating is displayed on an LCoS SLM. At normal incidence, the CA of the field reflected by the LCoS of a plane wave of amplitude A will be

$$\begin{aligned} U(x,y) &= A\exp\left\{ i\beta(x,y)\cos\left[2\pi u_0 x + \phi(x,y)\right]\right\} \\ &= A\exp\left[i\alpha(x,y)\right], \end{aligned} \tag{1}$$

where A is a real constant, u_0 is the spatial frequency of the grating, and $2\beta(x,y)$ and $\phi(x,y)$ are, respectively, the phase modulation depth and the phase modulation function of the grating. Equation (1) resemblances the Jacobi-Anger expansion [28],

$$\exp(iz\cos\theta)\sum_{n=-\infty}^{\infty} i^n J_n(z)\exp(in\theta),$$

(2)

where J_n is the Bessel function of the first kind and n th order, thus Eq. (1) can be rewritten as

$$U(x,y) = A\sum_{n=-\infty}^{\infty} i^n J_n[\beta(x,y)]\exp[in\phi(x,y)]\exp(in2\pi u_0 x)$$

(3)

so that, except for the constant factor i^n, the CA of the beam diffracted into the order +1 is

$$U_{+1}(x,y) = AJ_1\left[\beta(x,y)\right]\cdot\exp\left[i\phi(x,y)\right]. \tag{4}$$

If we wish to use $U_{+1}(x,y)$ to design a PhM with an equivalent CA transmittance

$$t(x,y) = a(x,y)\exp\left[i\phi(x,y)\right], \quad 0\le a(x,y)\le 1, \tag{5}$$

from Eqs. (4) and (5) follows that we must have

$$A\,J_1\left[\beta(x,y)\right] = a(x,y). \tag{6}$$

By construction, $a(x,y)$ is a bounded function; if we restrict the values of the phase $\beta(x,y)$ to those within the first half-lobe of $J_1[\beta(x,y)]$, $0\le\beta(x,y)\le 1.8412$, so $0\le J_1[\beta(x,y)]\le 0.5819$, then necessarily $A=1/J_1(\beta_{\max})$, where $\beta_{\max}\le 1.8412$ is the maximum value that can assume $\beta(x,y)$. With this in mind, Eq. (6) can be rewritten as

$$J_1\left[\beta(x,y)\right] - J_1\left(\beta_{\max}\right)\cdot a(x,y) = 0, \quad 0\le\beta(x,y)\le\beta_{\max}, \quad \beta_{\max}\le 1.8412. \tag{7}$$

For this work we chose $\beta_{\max}(x,y)=1.8412$, so that $J_1(\beta_{\max})=0.5819$.

If we add the phase $\phi_c(x,y)$ required to compensate the aberrations of the super-resolving system, including those introduced by the LCoS panel, from Eq. (1) follows that the phase we need to encode in the LCoS is:

$$\alpha(x,y) = \beta(x,y)\cos\left[2\pi u_0 x + \phi(x,y) + \phi_c(x,y)\right], \tag{8}$$

where $\beta(x,y)$ is obtained from Eq. (7), and $a(x,y)$ and $\phi(x,y)$ are given functions [Eq. (5)].

Apart from the case of a phase-only PhM [$a(x, y) = 1$], where $\beta(x, y) = \beta_{\max}$, the values of $\beta(x, y)$ must be obtained from Eq. (7) through a root-finding algorithm. Eq. (7) can in principle have multiple solutions, depending on the value of $a(x, y)$. For our purposes, however, those outside the first half-lobe of $J_1(\beta)$ would be irrelevant. The excursion of the phase $\alpha(x, y)$, then, will be at most $\pm \beta_{\max} = \pm\ 1.8412 \sim \pm\ 0.59\pi$ [Eq. (8)], or, equivalently, $[0,\ 1.18\pi]$. This phase interval was reachable with classic SLMs, which allowed a phase range $0 \le \alpha(x, y) \le 2\pi$, approximately. In short, with this encoding technique we only required about 59 % of the maximum phase shift provided by our LCoS.

To encode the phase $\alpha(x,y)$ in an LCoS, we display first in a personal computer monitor a 255 grayscale image $I(x,y)$ of the function $\alpha(x,y)$. In our case this had 1016×720 pixels - the number of pixels in our LCoS. Assuming for simplicity that $\phi(x,y) = 0$ and $\phi_c(x,y) = 0$, from Eq. (8) we would have

$$\begin{aligned} I(x, y) &= I_0 + \alpha(x, y) \\ &= I_0 + \beta(x, y)\cos\left(2\pi u_0 x\right) \\ &= I_0 + \beta_{\max} V(x, y)\cos\left(2\pi u_0 x\right), \end{aligned} \tag{9}$$

where I_0 is a constant and

$$V(x, y) = \frac{\beta(x, y)}{\beta_{\max}}, \quad 0 \le V(x, y) \le 1. \tag{10}$$

Evidently $V(x, y)$ is related to the visibility, or contrast, of the fringes in the pattern $I(x, y)$. Notice that

$$\begin{aligned} I(x, y)_{\max} &= I_0 + \beta_{\max} \le 255, \\ I(x, y)_{\min} &= I_0 - \beta_{\max} \ge 0. \end{aligned} \tag{11}$$

and thus

$$I(x, y)_{\max} - I(x, y)_{\min} = 2\beta_{\max}. \tag{12}$$

Therefore, the number of gray levels, or phase steps, assigned to $I(x, y)$ is proportional to $\beta_{\max}$. If $\beta_{\max} < 0.59\pi$, say $\beta_{\max} = 0.35\pi$, the number of phase steps at our disposal would be reduced from (1.18π/2π)×255 ~ 150 (~59%) to (0.70π/2π)×255 ~ 89 (~35%). In Fig. 1 are shown the graphs of $V(x, y)$ *vs* $a(x, y)$ for $\beta_{\max} = 0.59\pi$ (solid line) and $\beta_{\max} = 0.35\pi$ (dashed line) obtained from Eqs. (7) and (10). It is clear that the last yields a better mapping, but the price we

pay for this is less light in the +1 diffraction order of the phase grating, and a coarser sinusoidal profile, which will produce stronger diffracted fields of high spatial frequencies (noise).

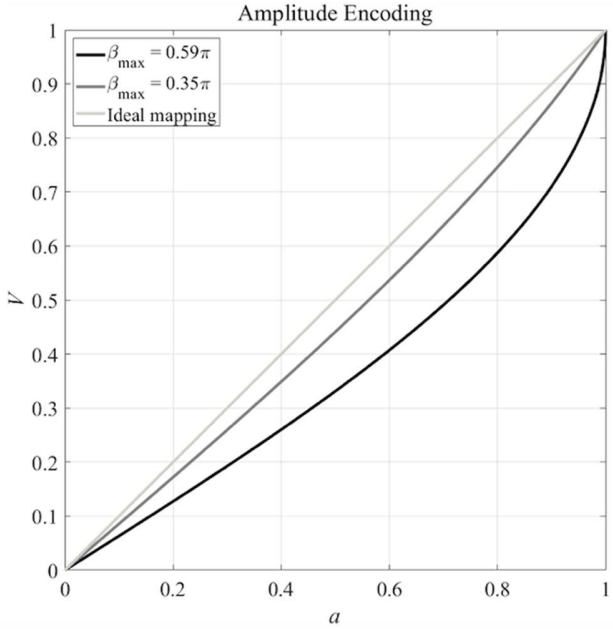

Fig. 1. Visibility V (contrast) in the hologram to be displayed in the LCoS *vs* the amplitude a of the PhM. When a ~1, the curve corresponding to $\beta_{max} = 0.59\pi$ (solid line) becomes very steep. This undesirable behavior can be avoided if we choose $\beta_{max} = 0.35\pi$ (dashed line), but the light in the +1 diffraction order would be less [Eq. (4)], and the sinusoidal phase grating profile in this case would be coarser.

Since $a(x, y)$ is variable, $\beta(x, y)$, and thus $V(x, y)$, would also be variables [Eqs. (7) and (10)]. When at some point of the LCoS $V(x, y)$ decreases, the amplitude $a(x, y)$ of the CA-PhM also decreases (Fig. 1). If $V(x, y) = 0$, there is no diffraction at that point and therefore the amplitude of the CA-PhM would be zero there. If in other point we shift the local fringes (phase modulation), the phase $\phi(x, y)$ of the PhM will change according to Eqs. (8) and (5).

The idea behind the coding procedure can be presented as follows. We start with an ordinary phase grating, *i.e.*, with a sinusoidal phase grating of constant phase depth and constant period. Let us vary the phase depth of every single pixel with respect to the original grating. The actual amplitude of the wave diffracted by every single pixel, $a(x, y)$, would depend on its new phase depth, $2\beta(x, y)$ [Eq. (7)] keeping the same orientation of the grooves. The new pixel's phase, relative to the phase of the wave diffracted $\phi(x, y)$ [Eq. (8)] by the original grating (order +1) [Ec. (4)], depend on the shift that we gave to the modified grating.

Thus, the amplitude $a(x, y)$ of the PhM is encoded as the visibility $V(x,y)$ of the fringes of the pattern $I(x,y)$ [29]. Next, this pattern is relayed to the LCoS to obtain a digitized, modulated phase grating with a CA reflectance

$$r(x,y) = r_0 \exp\left[i\alpha(x,y)\right] = r_0 \exp\left\{i\beta_{\max} \cdot V(x,y) \cos\left[2\pi u_0 x + \phi(x,y) + \phi_c(x,y)\right]\right\}, \qquad (13)$$

where r_0 is a constant. For simplicity, we shall refer to $I(x,y)$, the grayscale image of the phase $\alpha(x,y)$, as the hologram [Eq. (9)].

3. NUMERICAL VALIDATION

3.1 Complex amplitude phase mask

A numerical simulation was carried out to validate the complex-amplitude encoding method described above. A super-resolving, axially symmetric, CA-PhM, proposed by V. F. Canales and M. P. Cagigal [30], was encoded in a phase grating. The mask consisted of 5 annuli, delimited by the normalized radial coordinates $\rho_n =$ (0.098, 0.222, 0.238, 0.472, 1), $n =$ 1, 2, … ,5. The amplitude transmittances of these annuli were $a_n =$ (0.598, 0.712, 0.824, 0.955, 1); beyond the last annulus, the LCoS was diaphragmed, and thus we had $a(\rho) = 0$ for $\rho > 1$. The phases were alternatively π and 0: $\phi_n =$ (π, 0, π, 0, π) (see Fig. 2). The corresponding values of $V(\rho)$ were obtained from Eqs. (7) and (10), with $\beta_{\max} = 1.8412$. These were $V_n =$ (0.4056, 0.5017, 0.6137, 0.8061, 1). We used 33 fringes within a circle of 14 mm diameter, so that the value of the spatial frequency of the hologram was $u_0 = 2.36$ cycles/mm. Fig. 3 shows this hologram. Notice that phase variations are encoded as fringe dislocations, and amplitude changes as fringes of increasing contrast from the first to the last annulus.

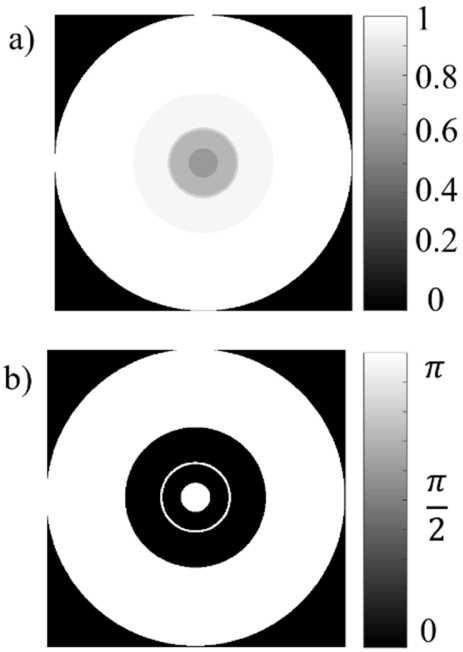

Fig. 2. Maps of Canales and Cagigal's complex-amplitude pupil mask: a) amplitude, b) phase [30].

To check that the previous CA-PhM acts indeed as a super-resolving pupil, we computed the corresponding point spread function (PSF):

$$\left|h(u,v)\right|^2 = \left|F\ \{t(x,y)\}\right|^2, \tag{14}$$

where $t(x,y)$ is given by Eq. (5), and F stands for Fourier transformation. The spatial frequencies (u,v) are related to the coordinates $\left(x_f, y_f\right)$ at the back focal plane of the lens L_1 through the equation

$$(u,v) = \left(x_f, y_f\right)\big/\lambda f\,. \tag{15}$$

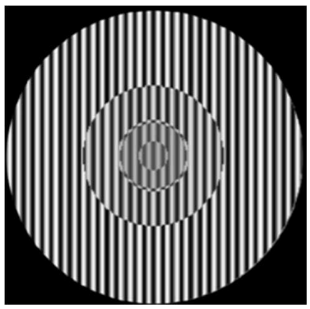

Fig. 3. Hologram of Canales and Cagigal's complex-amplitude pupil mask. Phase variations appear as fringe dislocations and amplitude changes as fringes of distinctive contrasts (visibilities) [30].

Fig. 4 shows with a solid line the section $\left|h(u,0)\right|^2$ of this PSF. For comparison, the normalized PSF of a diffraction-limited system, the so-called Airy intensity distribution, was included in the figure with a dashed line. The values of the abscissas in the plot are of x_f/r_1, where r_1 is the radius of the first zero of the Airy pattern. Notice that the super-resolving PSF has in fact a narrower central lobe, a mark of super-resolution, although, as expected, it is dimmer than the PSF of the clear pupil.

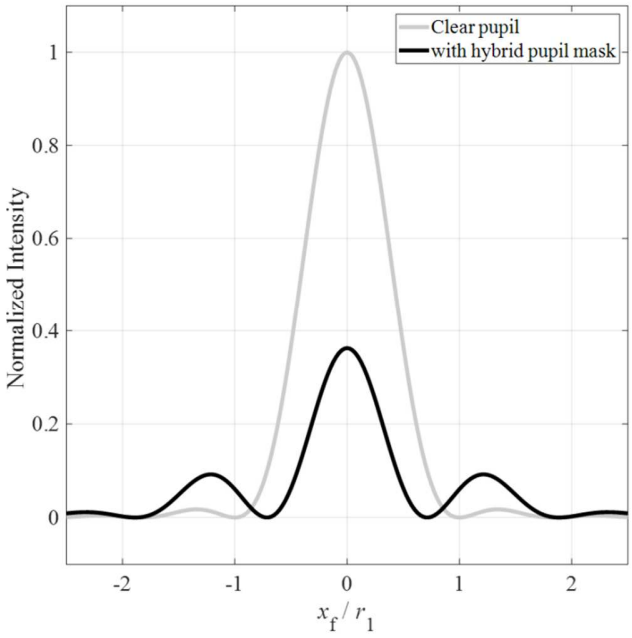

Fig. 4. Computed PSF for the CA-PhM encoded in the +1 diffractive order of the phase grating recorded with the hologram of Fig. 3 (solid line). The normalized PSF of a diffraction-limited system, the so-called Airy pattern, is shown for comparison with a dashed line. The values of the abscissas are of x_f / r_1, where r_1 is the radius of the first zero of the Airy pattern.

3.2 Influence of flicker in the PSF when using two SLMs

In this paper, we have shown that a complex filter can be implemented using only one phase spatial filter by encoding the amplitude into the visibility of a hologram. This complex filter can also be implemented using two different SLM, one acting as the phase component and the second one as an amplitude component. By superposing both components, the complex filter is achieved. However, these devices are well known to have an intrinsic flicker in the phase and or amplitude due to the move of the liquid crystal molecules.

It has been shown that the flicker can be modelled in a simplified version with a triangular function

$$\Gamma(t) = \begin{cases} \varphi_\Gamma - a_\Gamma + 2\frac{2a_\Gamma}{T/2}t & 0 \le t < \frac{T}{2} \\ \varphi_\Gamma + 3a_\Gamma - 2\frac{2a_\Gamma}{T/2}t & \frac{T}{2} \le t < T \end{cases}, \tag{16}$$

where φ_Γ is the retardance of the flicker fluctuation independent to each SLM panel. a_Γ corresponds to the fluctuation level. Polarimetric or physical methods can reduce the intrinsic flicker's level as already shown [17, 31]. We point out that in such a case, the flicker level is controlled, its retardance is exceptionally complicated to control. Let us model two different LCoS; each one has an amount of flicker and own transmittance.

$$\begin{aligned} t_1(x,y,t) &= a_1(x,y) + \Gamma_1(t) \\ t_2(x,y,t) &= \exp\left[i\left(\varphi(x,y) + \Gamma_2(t)\right)\right] \end{aligned}, \tag{17}$$

The transmittance of the panels is configured so that one SLM behaves as only-phase and the second one as an amplitude modulator. Moreover, it has to be noticed that the flicker function of each transmittance is different, and there is no way to synchronize the respective SLM's panel retardance $\varphi_{\Gamma_1}$and φ_{Γ_2}. For simplicity, we are assuming that both SLMs have the same level of fluctuation a_Γ. Thus, after superposing both transmittances, the resulting field can be expressed as

$$U_\Gamma(x,y,t) = [a_1(x,y) + \Gamma_1(t)]\exp\left[i\left(\varphi(x,y) + \Gamma_2(t)\right)\right]. \tag{18}$$

A simulation using Eq. 18 has been done using the same values of the complex filter as in section 3.1, a_Γ was set as a constant; nevertheless, it depends on the grey-level used by the spatial light modulator. Here, an amplitude of 0.001 volt/grey-level was chosen. The difference between the retardance of flicker in both SLMs was varied to look for effects in super-resolution. Here we express this difference as $\Delta\varphi_\Gamma = |\varphi_{\Gamma 2} - \varphi_{\Gamma 1}|$.

A temporal average in over one period was obtained in equation 18, and the resulting PSF computed.

$$h_\Gamma(u,v) = \langle |U_\Gamma(x,y,t)|^2 \rangle_T \tag{19}$$

Where $\langle\,.\,\rangle$ corresponds to the average through the whole period of the flicker function. In Fig. 5, the effect over the PSF when two different SLM are not synchronized is shown. The PSF shows a degradation in amplitude and resolution, as the Strehl ratio of the function is reduced. In Figure 5b, it can be seen that, when the respective SLM flicker is not in phase super-resolution is not achieved, or in the best case, flicker could provoke a certain error.

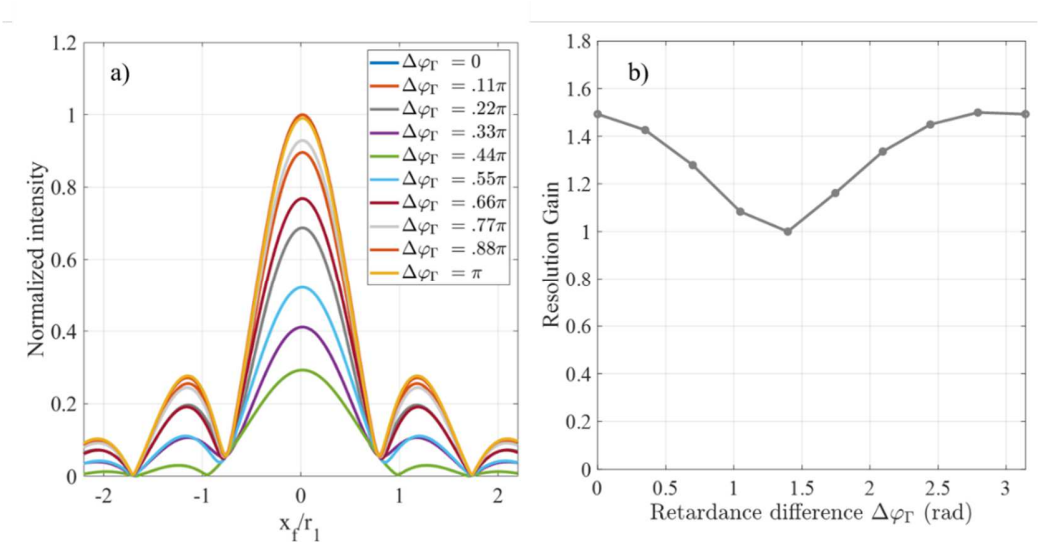

Fig. 5. Effect of the flicker when two unsynchronized LCoS are used in super-resolution complex filters. a) deterioration of the PSF, b) Deterioration of the resolution gain (normalized with the Airy pattern).

4. EXPERIMENTAL SETUP AND RESULTS

Fig. 6 shows the experimental setup that was used to record super-resolving PSFs. The beam of a He-Ne laser (L), $\lambda = 633$ nm, was expanded by a $25\times$ microscope objective (MO), a spatial filter (SF) and a 250 mm focal length collimating lens (L_0). The SLM was a twisted nematic LCoS from Holoeye, model LC-R 2500. To bound the pupil area, a 14 mm diameter diaphragm (D) was placed in front of the LCoS. This diameter was equal to the height of the LCoS rectangular aperture of $20\times14\ \text{mm}^2$, and corresponded thus to the largest circle that could be inscribed on it.

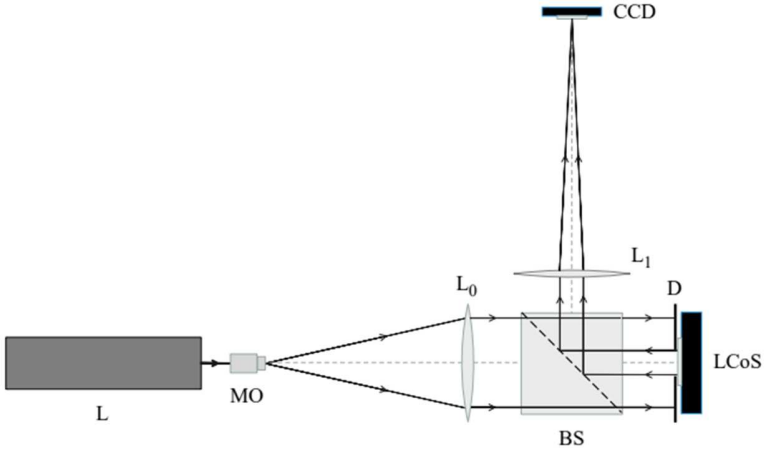

Fig. 6. Schematic diagram of the experimental setup. L is a He-Ne laser λ = 633 nm ; MO a $25\times$ microscope objective; L_0 and L_1 are lenses of 250 and 1,000 mm focal length, respectively; BS is a beam splitter; D a 14 mm diameter diaphragm; LCoS a 1016×720 pixels liquid crystal on silicon SLM; and CCD a charge-coupled device with pixels of 5.2×5.2 μm^2.

To observe a super-resolving PSF, we had to focus on a charge-coupled device (CCD) the beam diffracted by the LCoS and reflected by the beam splitter (BS), using a 1,000 mm focal length lens (L_1). When doing this, it was essential that the focused beam was free from off-axis aberrations, basically coma and astigmatism, as well as spherical aberration. If the aberrations of the LCoS are compensated, the first could be averted if the ray through the center of the diaphragm D, after being diffracted by the LCoS into the +1 diffraction order, and reflected by the BS, coincides with the optical axis of the lens L_1. Spherical aberration would be negligible if the focal ratio of the focusing beam were very large; it was for this reason that we chose L_1 with a large focal length. In the present case, this focal ratio was ~*F*/70. Additionally, this arrangement magnifies sufficiently the PSFs to be resolved by the CCD, which was from a Lumenera M-LU175 camera and had a pixel size of $5.2\times5.2\ \mu\text{m}^2$. The radius of the first zero of the Airy pattern in the focal plane of L_1 is

$$r_1 = 1.22\frac{\lambda}{D}f = 1.22(F/\#)\lambda. \tag{20}$$

In the present case, $\lambda = 0.633 \times 10^{-3}$ mm, $D = 14$ mm and $f = 1000$ mm. Therefore, the diameter of the central lobe of the pattern was $2r_1 \sim 110$ μm. Summarizing, to observe a super-resolving PSF, it is crucial to form a relatively large, virtually aberration-free PSF. Otherwise, its potential super-resolving features would be lost.

A. Spatial Light Modulator calibration

Since the LCoS panel is thin, it is inevitable that it will have slight deformations that will spoil a potential super-resolving PSF, even if these deformations are small. At the top of Fig. 7 is shown an interferogram of our LCoS panel, obtained with a WYKO 6000 digital Fizeau interferometer. The deformation of the panel is evident. Using the raw data files from the interferometer, we can map this deformation in μm, change their sign, and inject them back into the LCoS, following the procedure described in [23]. This is a recursive procedure, in which we consecutively test the wavefront emerging from the +1 diffraction order of a phase grating displayed in the LCoS, something that is physically attained by the proper (small) tilt of the LCoS. We will end up with a phase-modulated phase grating [Eq. (13)], like those shown in Fig. 8. In the second row of Fig. 7 we can see the initial phase map obtained from the LCoS, and the subsequent maps with phase corrections obtained from the +1 diffraction order of the phase grating displayed by this. The third row shows the PSFs corresponding to these maps. Since an LCoS panel is rectangular, the appearance of the PSFs approaches that of $\mathrm{sinc}^2\left(l_x u, l_y v\right)$, where u and v are spatial frequencies [Eq. (15)], and l_x and l_y are the length and the height of the LCoS panel [32].

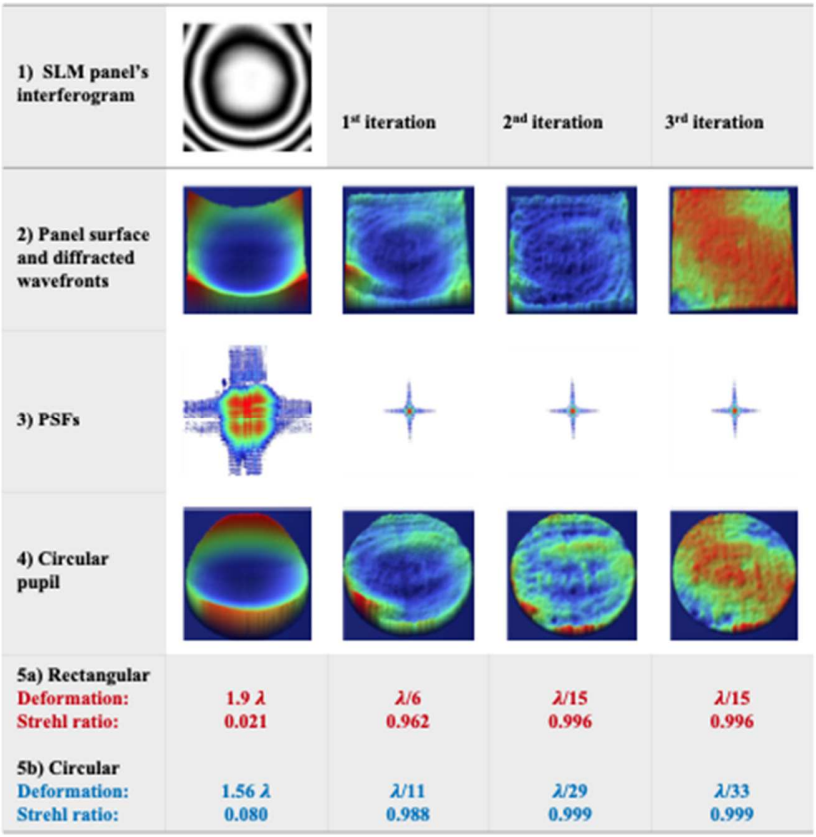

Fig. 7. The LCoS panel aberrations were corrected in three measurement iterations, as shown in the second row. Their PSFs appear below, in the third row. A circular pupil contained in the LCoS rectangular aperture is shown in the fourth row. The correction within the rectangular aperture of the LCoS reached $\lambda/15$, and within the circular aperture $\lambda/33$, as shown in row 5. Notice that in both apertures the final Strehl ratio is virtually 1.

The fourth row of Fig. 7 shows the phase maps for the circular aperture in successive iterations. Limiting the LCoS aperture to a circular aperture will, of course, improve the correction achieved in each cycle, because we will remove the largest residual deformations, which are in the panel edges. Finally, in the fifth row of Fig. 7 we show the peak-to-valley (P-V) deformations and Strehl ratios for the successive rectangular (in red) and circular (in blue) phase maps, with the P-V deformations given as fractions of the wavelength, $\lambda = 633$ nm. Notice that these values are well below $\lambda/14$, Marechal's condition for a well corrected optical system [22].

Fig. 8 shows our hologram (Fig. 3) after compensation of the panel aberrations. As we mentioned above, this was achieved by adding the correction phase $\phi_c(x,y)$ to $\alpha(x,y)$, the phase of the grating that will display the LCoS [Eq. (8)]. It should be mentioned that, in principle, the aberrations of the entire optical system in Fig 6 could be, if necessary, compensated in this form.

Fig. 8. The hologram of Fig. 3 after including the phase correction term ϕ_c to compensate the aberrations introduced by the LCoS.

B. Observed super-resolving PSFs

Fig. 9a and b show two experimental PSFs recorded with a CCD; the first one has been obtained with a clear pupil and the second one with the super-resolving pupil. The clear pupil is aberration-corrected by the LCoS ϕ_c. Its output beam travels the same optical path and has the same numerical aperture as the complex PhM so that it can be appropriately compared.

Their central horizontal section of these PSFs are shown in Fig. 10a and b, the first with a gray line, and the second with a black one. As expected, the lobe of the second PSF is narrower than the first, and the first PSF is brighter than the second.

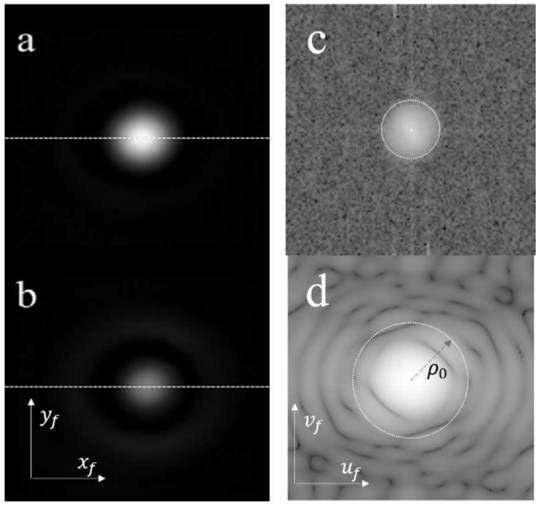

Fig. 9. Experimental point spread functions and computed modulation transfer function. a) Airy distribution, b) super-resolving PSF obtained with the +1-diffraction order, c) MTF of the Airy distribution, d) MTF with the hybrid phase mask

The Fourier transform of the Figures 9a and b can be seen in Figures 9c-d. The Fourier transformation of the PSF corresponds to the modulation transfer function (MTF). MTF lets us determine the cutoff frequency of the system ρ_o. The radial average of the MTF is displayed in

Fig 10b, where the complex filter MTF (black line) is compared with the MTF of a clear pupil (gray line). Note that artifacts beyond the cutoff frequency are due to the FFT algorithm. As expected from the PSF, the frequency gain is notorious, and the cut off frequency has been incremented. The spatial frequency has been normalized to the clear pupil cutoff frequency.

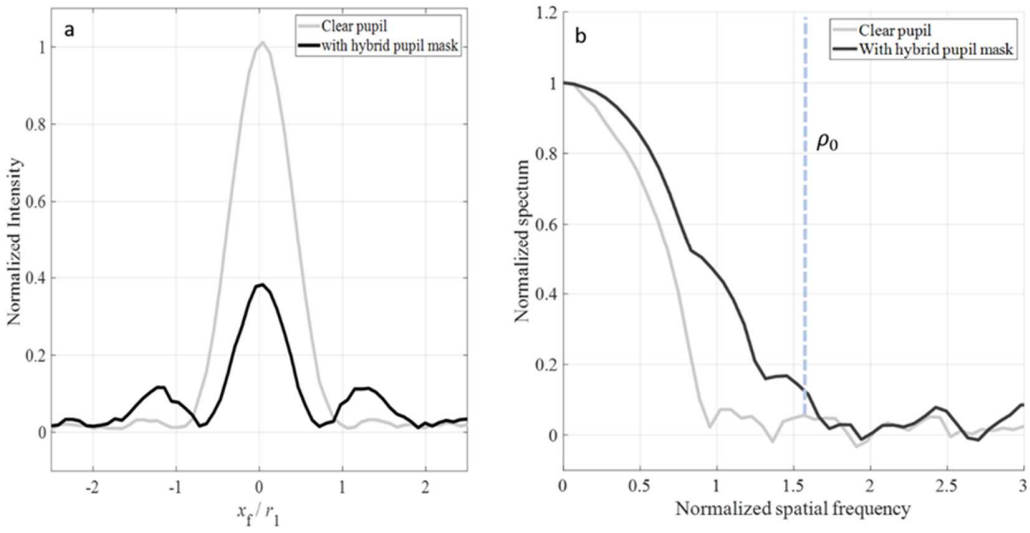

Fig. 10. Horizontal central sections in Fig. 9 a) Experimental PSF, b) Radial average of the MTF.

5. CONCLUSIONS

We described a method to design super-resolving PhMs that requires only one, phase-only, SLM. This method allows the generation of CA-PhMs by means of a phase grating displayed in an LCoS SLM. We showed that the aberrations introduced by this device can be successfully compensated in this grating, with residual aberrations bellow $\lambda/14$, the condition that must satisfy a well corrected optical system according to Maréchal [22]. However, this can only be achieved after an interferometric calibration of the panel flatness of the LCoS, which we did with a digital Fizeau interferometer.

There are improvements, of course, that can be made to this technique of producing super-resolving masks. Their phase encoding is simple, not so much the amplitude encoding. In the case presented here, $\beta_{max} \leq 1.8412$. When $a(x,y) \sim 1$, the mapping of the PhM amplitude to the visibility (contrast) of the fringes in the grayscale image $I(x,y)$ that is relayed to the LCoS is highly non-linear [Fig. 1]. This drawback can be surmounted if we reduce the maximum phase depth of the grating, $2\beta_{max}$, in the LCoS [Eq. (13)], although this would reduce as well the amount of light intended for the super-resolving image.

The phase flicker of LCoS SLM devices that appeared as a biting phenomenon when superposing two different pupils has been overcome by generating a complex-amplitude phase mask in a single phase-only SLM.

AKNOWLEDGEMENTS

J. E. A. Landgrave is indebted to Abundio Dávila, from Centro de Investigaciones en Óptica, for discussions on the technicalities of the LCoS SLM.

REFERENCES

1. Abbe E. Beiträge zur Theorie des Mikroskops und der mikroskopischen Wahrnehmung. Arkiv Mikroskop Anat 1873; 9: 413–468.

2. Sales TRM. Smallest Focal Spot. Phys Rev Lett 1998; 81(18): 3844-3847.

3. Gustafsson MG. Surpassing the lateral resolution limit by a factor of two using structured illumination microscopy. J Microscopy 2000; 198(2): 82–87.

4. Hell SW, Wichmann J. Breaking the diffraction resolution limit by stimulated emission: stimulated-emission-depletion fluorescence microscopy. Opt Lett 1994; 19(11): 780–782.

5. Rust MJ, Bates M, Zhuang X. Sub-diffraction-limit imaging by stochastic optical reconstruction microscopy (STORM). Nat Methods 2006; 3: 793-796.

6. Dyba M, Hell SW. Focal spots of size λ/23 open up far-field florescence microscopy at 33 nm axial resolution. Phys Rev Lett 2002; 88(16): 163901 1-4.

7. Aguilar A, Dávila A, García-Márquez J. Multi-step vortex filtering for phase extraction. Opt. Express 2014; 22(7): 8503-8514.

8. Tzang O, Feldkhun D, Agrawal A, Jesacher A, Piestun R. Two-photon PSF-engineered image scanning microscopy. Opt Lett 2019; 44(4): 895–898.

9. Huang X, Fan J, Li L, *et al*. Fast, long-term, super-resolution imaging with Hessian structured illumination microscopy. Nat Biotechnol 2018; 36: 451-459.

10. Gustavsson A, Petrov PN, Lee MY, *et al*. 3D single-molecule super-resolution microscopy with a tilted light sheet. Nat Commun 2018; 9: 123.

11. Cagigal MP, Canales VF, Oti JE. Design of Continuous Superresolving Masks for Ground-based Telescopes. Publ Astron Soc Pac 2004; 116: 965-970.

12. Toraldo di Francia G. Super-Gain Antennas and Optical Resolving Power. Nuovo Cimento 1952; 9(S-3): 426–438.

13. Márquez A, Iemmi C, Escalera JC, Campos J, Ledesma S, Davis JA, Yzuel M, Amplitude apodizers encoded onto Fresnel lenses implemented on a phase-only spatial light modulator, Appl Opt 2001; 40(14): 2316-2322.

14. Gundu PN, Hack E, Rastogi P. High efficient superresolution combination filter with twin LCD spatial light modulators. Opt Express 2005; 13(8): 2835–2842.

15. Gundu PN, Hack E, Rastogi P, 'Apodized superresolution'–Concept and simulations. Opt Comm 2005; 249: 101-107.

16. Kowalczyk AP, Makowski M, Ducin I, Sypek M, Kolodziejczyk A. Collective matrix of spatial light modulators for increased resolution in holographic image projection. Opt Express 2018; 26(13): 17158–17169.

17. García-Márquez J, López V, González-Vega A, Noé E. Flicker minimization in an LCoS spatial light modulator. Opt Express 2012; 20(8), 8431– 8441.

18. Márquez A, Martínez-Guardiola FJ, Francés J, Ramírez MG, Calzado EM, Morales-Vidal M, Gallego S, Pascual I, Blazed grating theory to minimize the non-idealities in LCoS devices. Proc SPIE 2019; 11136: 1113613(1-7).

19. Márquez A, Moreno I, Iemmi C, Lizana A, Campos J, Yzuel MJ. Mueller-Stokes characterization and optimization of a liquid crystal on silicon display showing depolarization. Opt. Express 2008; 16(3): 1669–1685.

20. Calderón-Hermosillo Y, García-Márquez J, Espinosa-Luna R, Alcalá Ochoa N, López V, Aguilar A, Alayli Y. Flicker in a twisted nematic spatial light modulator. Opt Lasers Eng 2013; 51(6): 741–748.

21. Yang H, Chu DP. Phase flicker optimisation in digital liquid crystal on silicon devices. Opt Express 2019; 27(17): 24556–24567.

22. Born M, Wolf E. Principles of Optics. Chap 9. 7th ed. Cambridge: Cambridge University Press; 1999.

23. García-Márquez J, Landgrave JEA, Alcalá-Ochoa N, Pérez-Santos C. Recursive wavefront aberration correction method for LCoS spatial light modulators. Opt Lasers Eng 2011; 49(6): 743–748.

24. López V, González-Vega A, Aguilar A, Landgrave JEA, García-Márquez J. Non-uniform spatial response of the LCoS spatial light modulator. Opt Commun 2016; 366: 419–424.

25. García-Márquez J, Alcalá N, Montoya M, Pérez C, Gutiérrez M, Moya J. Calibración de un interferómetro fizeau: cálculo de incertidumbres. Rev Mex Fis 2005; 51(1): 114–120.

26. Lizana A, Moreno I, Márquez A, Also E, Iemmi C, Campos J, Yzuel MJ. Influence of the temporal fluctuations phenomena on the ECB LCoS performance. Proc SPIE 2009; 7442: 74420G.

27 Márquez A, Martínez FJ, Gallego S, Ortuño M, Francés J, Beléndez A, Pascual I. Static and dynamic effects of flicker in phase multilevel elements on LCoS devices. Proc SPIE 2015: 9598; 95980C.

28. Weisstein EW. Jacobi-Anger Expansion. A Wolfram Web Resource. MathWorld. http://mathworld.wolfram.com/Jacobi-AngerExpansion.html

29. García-Márquez J, Instrumentations optiques inférieures à la limite de diffraction. Thesis of Habilitation à diriger des recherches. Université de Versailles Saint-Quentin: tel-01535141 version 1; 2013.

30. Canales VF, Cagigal MP. Pupil filter design by using a Bessel functions basis at the image plane. Opt Express 2006; 14: 10393–10402.

31. Yang H, Chu DP. Phase flicker in liquid crystal on silicon devices. J. Phys. Photon 2020; 2: 032001

32. Goodman JW. Introduction to Fourier Optics. Chap 4. New York: McGraw-Hill; 1968.